

Evaluation of off-angle thermal spray

S.H. Leigh, C.C. Berndt *

Thermal Spray Laboratory, Department of Materials Science and Engineering, State University of New York at Stony Brook,
Stony Brook, NY 11794-2275, USA

Received 16 May 1995; accepted 19 January 1996

Abstract

The effect of spray angle on the properties of plasma spray deposits has been investigated. Two different materials, NiAl and $\text{Cr}_3\text{C}_2\text{-NiCr}$, were sprayed at angles from 50 to 90° with respect to the substrate. The spray angle influenced the microstructure and the properties of the deposits. The porosity increased as the spray angle decreased, i.e. as the angle was shifted away from the perpendicular position. The surface roughness of the $\text{Cr}_3\text{C}_2\text{-NiCr}$ deposit was not sensitive to the spray angle, whereas NiAl exhibited an increase as the spray angle decreased. Microhardness, tensile adhesion strength, and interfacial fracture toughness decreased with spray angle. The change of these properties with spray angle is attributed to (1) the morphology of the splats, (2) the change of the local spray angle, and (3) the change of momentum of particles impacting on the substrate or previously deposited particles. The mechanical-property variations arise from porosity changes which occur from the spray angle variations. © 1997 Elsevier Science S.A.

Keywords: Mechanical properties; Porosity; Splat morphology; Spray angle; Spray pattern; Thermal spray

Nomenclature

$P(x)$	Gaussian probability distribution function
σ	standard deviation
μ	mean
α	spray angle (degrees)
$P'(x, \alpha)$	probability distribution function with spray angle α
σ_{90}	standard deviation at a 90° spray angle
d	spray distance (mm)
μ_3	skewness
P_x	spreading momentum
P_y	impacting momentum
m	Weibull modulus
X_0	characteristic strength
G_C	critical strain energy release rate (J m^{-2})
K_{IC}	fracture toughness ($\text{N m}^{-3/2}$)
P_C	fracture force (N)
D	outside diameter of the circumferentially notched bar (m)
d	inside diameter of the circumferentially notched bar (m)

1. Introduction

The thermal spraying process is controlled by numerous parameters which have a direct influence on the properties of the deposit. The sprayed deposits are often not reproducible between laboratories or factories

because it is difficult to maintain all of the processing parameters which are related to the properties of deposits. In addition, there are factors which are often ignored; for example, the spray angle is usually assumed to be 90° to the substrate.

The evaluation of thermally sprayed deposits is mostly carried out using coupons sprayed at 90°¹. The engineering component, however, sometimes requires spraying at angles other than 90°. This aspect would be notable when no automation was used during the spray process, since it is not easy to maintain a torch at right angles to a three-dimensional substrate. The property of "off-angle spraying" is becoming an important aspect as the demand of spraying complex-shaped parts increases, especially in the thermal spray forming area. Moreover, Fasching et al. [1] recently reported that asymmetries of spray distribution can be corrected by tilting the spray torch so that uniformly thick deposits can be built up. Such off-angle spraying may also change the structure and properties of coatings.

Hasui et al. [2] studied the effect of spray angles

¹The reference angle of 90° denotes an arbitrary reference where the torch axis is perpendicular to the substrate. Angles less than 90° will align the torch axis parallel to the substrate such that at 0° virtually no particles impact the substrate.

* Corresponding author.

ranging from 90 to 45° on the properties of molybdenum and alumina coatings. The porosity and surface roughness increased with the decrease of the spray angle, although only a slight change in porosity was reported. The adhesion and cohesion strengths were found to increase as the spray angle decreased, and deposition efficiency decreased with a decrease in spray angle. The morphology of splats was observed to vary with spray angle, i.e. the deposit splats tended to orient on the plane perpendicular to the spray direction. The properties of coatings sprayed at the angles down to 45° were not inferior to coatings sprayed at 90°.

Tucker and Price [3] also reported data dealing with the influence of spray angles on the mechanical properties of tungsten carbide-cobalt-based materials. They also observed similar microstructural changes with spray angle and found that there was no significant change in wear properties with spray angle.

In the current research, tests have been performed to characterize the properties of off-angle sprayed deposits, as well as a mathematical modeling of spray patterns which may be employed to optimize spraying processes in the spray-forming of complex-shaped parts.

2. Model of off-angle spraying

2.1. Macroscopic analysis

Materials deposited by thermal-spray processing exhibit a mass distribution across the substrate. This distribution, in the first instance, can be approximated by a Gaussian distribution. Fig. 1 depicts a typical configuration of a thermal spray system which shows the gun, spray jet, powder feeder, target and particle trajectory. It is assumed that the spray pattern is conical and symmetrical with the centerline of the torch. When the spray gun is tilted, the distribution of deposited materials would deviate from the Gaussian distribution.

The Gaussian probability distribution function $[P(x)]$

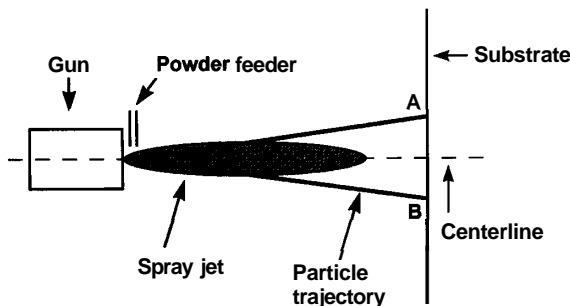


Fig. 1. Typical configuration of thermal spraying.

is expressed as:

$$P(x) = \frac{1}{\sqrt{\pi}\sigma} \exp\left[-\frac{(x-\mu)^2}{2\sigma^2}\right], \quad -\infty < x < \infty \quad (1)$$

where σ is the standard deviation and μ is the mean. In the case of spraying at 90° it is convenient to set μ to zero.

Fig. 2 shows the geometry of the spray process with a spray torch tilted by an angle α . For a certain spray angle α , the above equation can be transformed into a general form as a function of x and α (see Appendix A):

$$P'(x, \alpha) = \frac{1}{\sqrt{2\pi}\sigma_{90}} d^2 \frac{\cos(90-\alpha)}{[d-x\sin(90-\alpha)]^2} e^{-\frac{\left[\frac{dx\cos(90-\alpha)}{d-x\sin(90-\alpha)}\right]^2}{2\sigma_{90}^2}} \quad (2)$$

where α is the spray angle, σ_{90} is the standard deviation at a 90° spray angle, and d is the spray distance. Fig. 3 shows simulated distributions of spray deposits for spray angles from 90 to 30° when the stand-off distance (d) was 240 mm and the diameter of the perpendicular section through the cone at the substrate (line AB in Fig. 2) was 60 mm. This analysis assumed that the deposition efficiency was not influenced by the angle of particle impact, i.e. the area under each curve was unity. As will be shown later, these distributions would not exhibit equal areas at non-orthogonal angles. Thus, the cone angle can be determined as 14° and the standard deviation of the deposit pattern (or "spray print") at a 90° spray angle is 30.6 mm (see Appendix A).

In practical situations, these parameters vary with gun types and spray parameters. Furthermore, the particle trajectory centerline does not necessarily coincide with the torch centerline but shifts to either side [1,4]

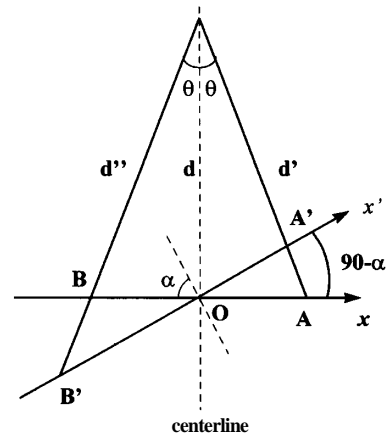


Fig. 2. Schematic of spray geometry. The torch is aligned along the dashed centerline, while the substrate orientation varies from AB to A'B' at angles α with respect to the normal orientation.

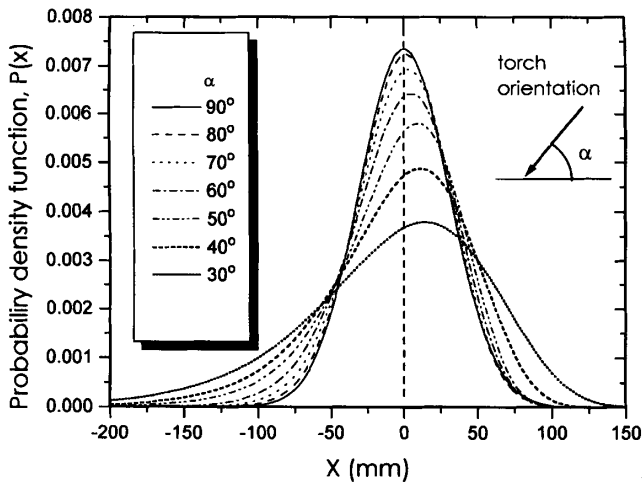


Fig. 3. Probability distribution of spray pattern for seven spray angles.

and the mass flux at the edge of the spray pattern would be diminished since the **unmelted/resolidified** particles would tend to rebound from the substrate. The deposit patterns at less than a 90° spray angle showed an asymmetry which increased as the spray angle decreased. The mean (μ) and the skewness (μ_3) are defined as:

$$\mu = \int_{-\infty}^{\infty} xP'(x,\alpha) dx \quad (3)$$

$$\mu_3 = \frac{\int_{-\infty}^{\infty} (x - \mu)^3 P'(x,\alpha) dx}{\sigma^3} \quad (4)$$

The mean value varied with the spray angle (Fig. 4), i.e. the centroid of the mass of the deposit pattern deviated from the centerline of the torch as the spray angle decreased. The skewness, which describes the symmetry of the mass distribution (see Fig. 3), of 90° deposit pattern was 0 and decreased with the spray angle (Fig. 5).

The spray distance is a critical spray parameter in

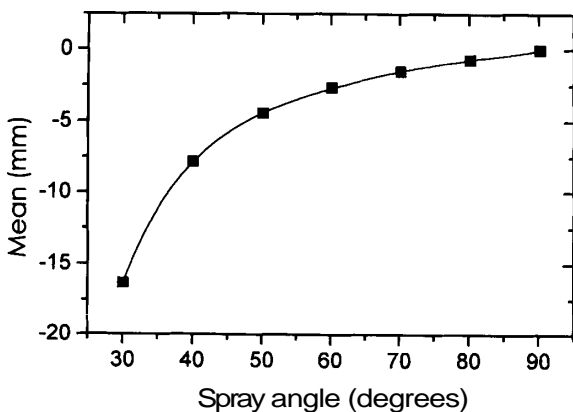


Fig. 4. Mean values of spray pattern distribution for different spray angles (90° is the optimum spray angle).

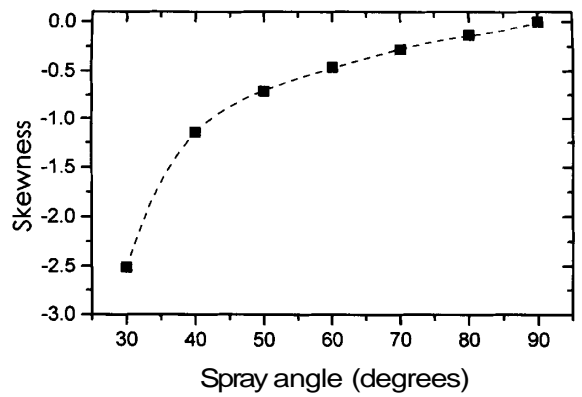


Fig. 5. Skewness of spray pattern distribution for different spray angles (90° is the optimum spray angle).

determining the property of sprayed deposits. The "local spray distance" gradually decreases from point B' to A' (on vector x' of Fig. 2) and the difference of the spray distance between the two points became larger as the spray angle (α) decreased. In Fig. 6 the local spray distance arising from off-angle spraying is normalized with respect to the torch centerline distance. This simple calculation indicated a -15 to +23% change in the optimum spray distance for the ± 30.6 mm spray print of the 50" torch-substrate orientation. Thus, the smaller spray angle would yield a more inhomogeneous deposit. This effect can be neglected at high spray angles (say, from 90 to 80°) because the conical spray jet produces a slight variance of spray distance from point A to B or A' to B'.

2.2. Microscopic analysis

The morphology of splats changes with respect to spray angle. [5,6] An example is illustrated in Fig. 7, where a molten particle impacts the substrate at an

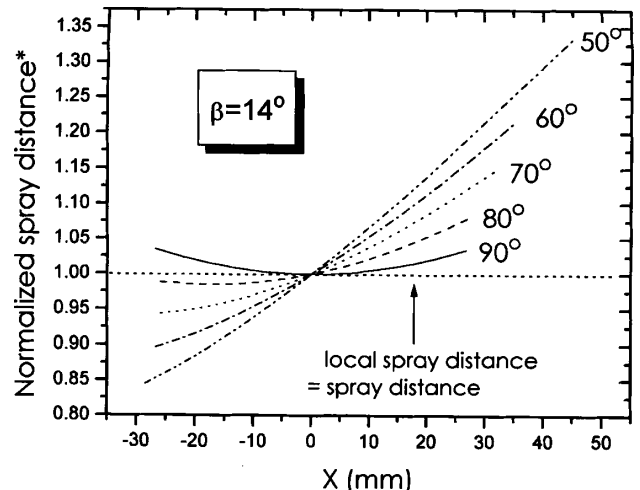


Fig. 6. Variation of local spray distance with different spray angles. *Normalized spray distance=local spray distance/spray distance.

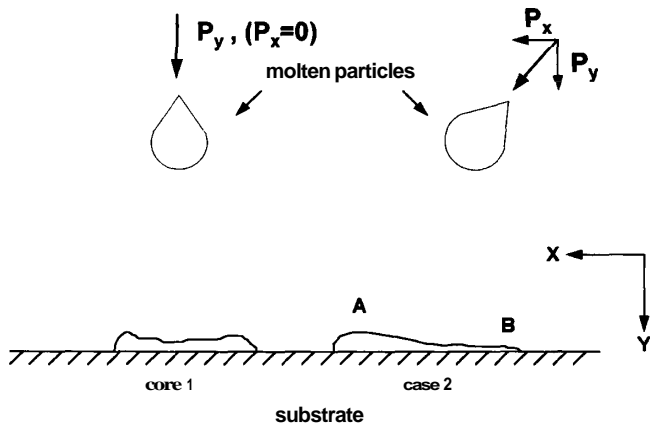


Fig. 7. Splat formation model.

angle other than 90° , i.e. if Cartesian coordinates are introduced, the particle impacts the substrate with x and y components of momentum P_x and P_y , respectively, whereas the particle traveling perpendicular to the substrate has a zero x component, i.e. $P_x=0$. The P_x component promotes particle spreading over the substrate rather than impacting on the substrate, and thus a thin and flat splat is created, i.e. P_x can be identified as a "spreading" momentum and P_y as an "impacting" momentum. The P_y component is smaller than that of a 90° impacting particle because the overall energy is divided into two components rather than one. Therefore, the deposit porosity would be expected to change with respect to spray angle (see Section 4.1 because the particles of low P_y do not impact the substrate with a sufficiently high momentum to consolidate the thermal spray coating structure. An asymmetric splat morphology is expected to occur because P_x contributes to the spreading of unsolidified materials toward point A (Fig. 7) during the solidification process. This phenomenon is dependent on material properties such as substrate surface roughness, substrate temperature, heat conductivity of substrate and solidification kinetics. [2, 7-9] A rough substrate, for example, would prevent particles from spreading, and ceramic materials with high melting points would spread less than metals before solidification.

3. Experimental procedure

3.1. Materials and sample preparation²

Two materials, NiAl (Metco 450NS) and Cr_3C_2 -NiCr (Metco 81VFNS), were sprayed onto steel substrates to determine the influence of the spray angles on characteristics of the thermal spray coatings. The NiAl was prepared at subsonic and Cr_3C_2 -NiCr at supersonic

(Mach 2) velocity. The spray equipment was a Miller Thermal SG-100[®] plasma gun and model 3620 control console. The chemical compositions of the feedstock materials are given in Table 1. The particle size distribution was measured using MicroTrac[®] equipment (Fig. 8).

Ten samples were sprayed onto disk-shaped substrates (25.4 mm (1 in) diameter and 6.4 mm (0.25 in) thick) for tensile adhesion tests (TATs) and on 25.4 mm (1 in) x 31.8 mm (1.25 in) panels for surface roughness, hardness, and metallography at angles of 50, 60, 70, 80 and 90° for both NiAl and Cr_3C_2 -NiCr.

3.2. Surface roughness test

The arithmetical average [10] of the coatings was measured using a SurfTest III[®] profilometer (Mitutoyo

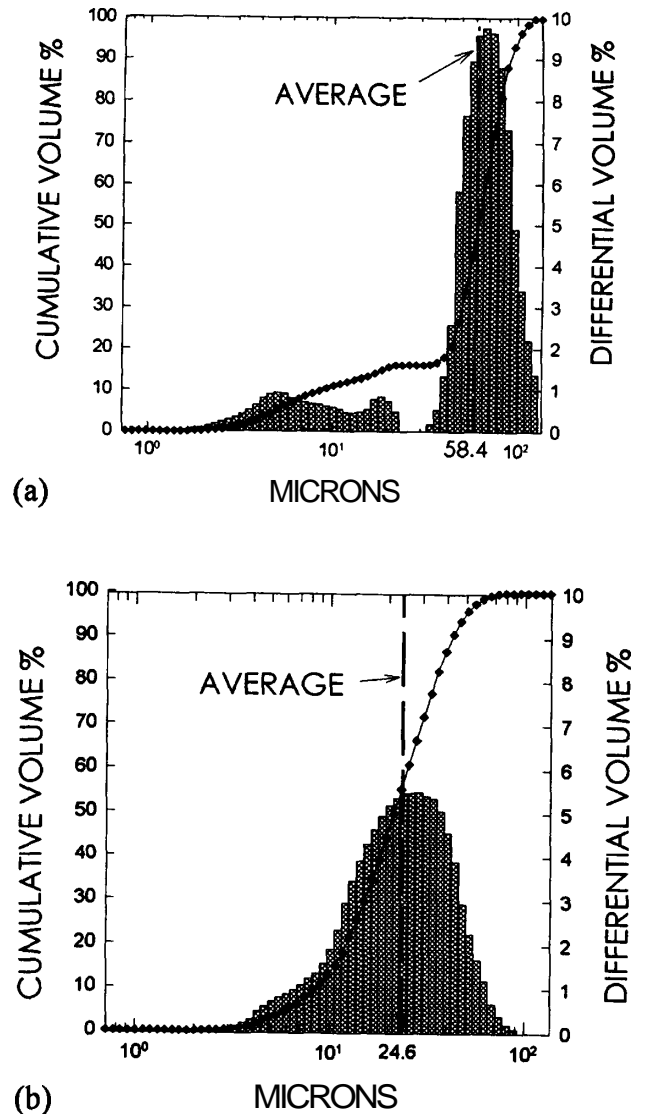


Fig. 8. Particle size distribution of (a) NiAl and (b) Cr_3C_2 -NiCr powders (the bimodal distribution for the NiAl composite powder arises from de-adhesion of the aluminum particles from the nickel core).

²This study was conducted on materials supplied by Metco, Inc. This company is now known as Sulzer-Metco, Inc.

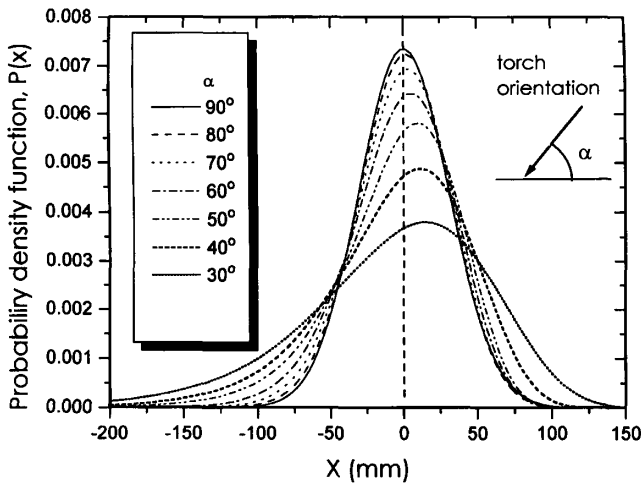


Fig. 3. Probability distribution of spray pattern for seven spray angles.

and the mass flux at the edge of the spray pattern would be diminished since the unmelted/resolidified particles would tend to rebound from the substrate. The deposit patterns at less than a 90° spray angle showed an asymmetry which increased as the spray angle decreased. The mean (μ) and the skewness (μ_3) are defined as:

$$\mu = \int_{-\infty}^{\infty} xP'(x,\alpha) dx \quad (3)$$

$$\mu_3 = \frac{\int_{-\infty}^{\infty} (x-\mu)^3 P'(x,\alpha) dx}{\sigma^3} \quad (4)$$

The mean value varied with the spray angle (Fig. 4), i.e. the centroid of the mass of the deposit pattern deviated from the centerline of the torch as the spray angle decreased. The skewness, which describes the symmetry of the mass distribution (see Fig. 3), of 90° deposit pattern was 0 and decreased with the spray angle (Fig. 5).

The spray distance is a critical spray parameter in

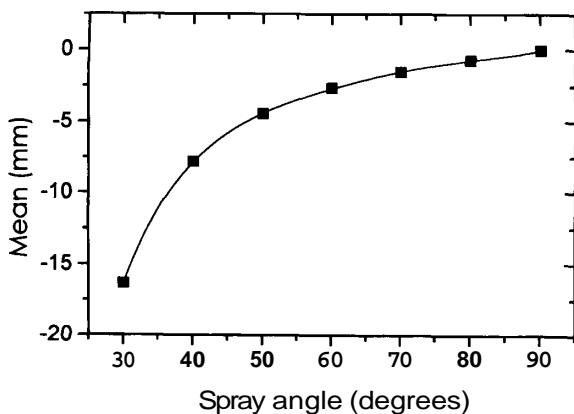


Fig. 4. Mean values of spray pattern distribution for different spray angles (90° is the optimum spray angle).

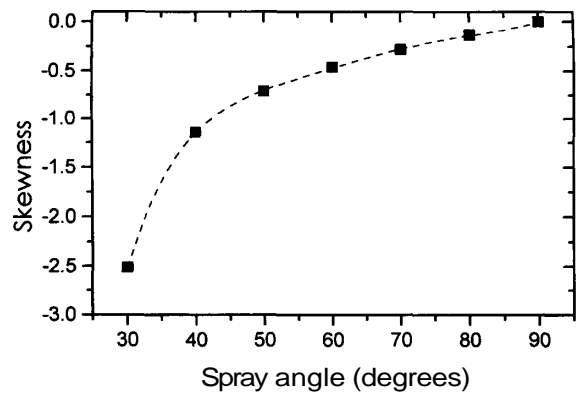


Fig. 5. Skewness of spray pattern distribution for different spray angles (90° is the optimum spray angle).

determining the property of sprayed deposits. The "local spray distance" gradually decreases from point B' to A' (on vector x' of Fig. 2) and the difference of the spray distance between the two points became larger as the spray angle (α) decreased. In Fig. 6 the local spray distance arising from off-angle spraying is normalized with respect to the torch centerline distance. This simple calculation indicated a -15 to +23% change in the optimum spray distance for the ± 30.6 mm spray print of the 50° torch-substrate orientation. Thus, the smaller spray angle would yield a more inhomogeneous deposit. This effect can be neglected at high spray angles (say, from 90 to 80°) because the conical spray jet produces a slight variance of spray distance from point A to B or A' to B'.

2.2. Microscopic analysis

The morphology of splats changes with respect to spray angle. [5,6] An example is illustrated in Fig. 7, where a molten particle impacts the substrate at an

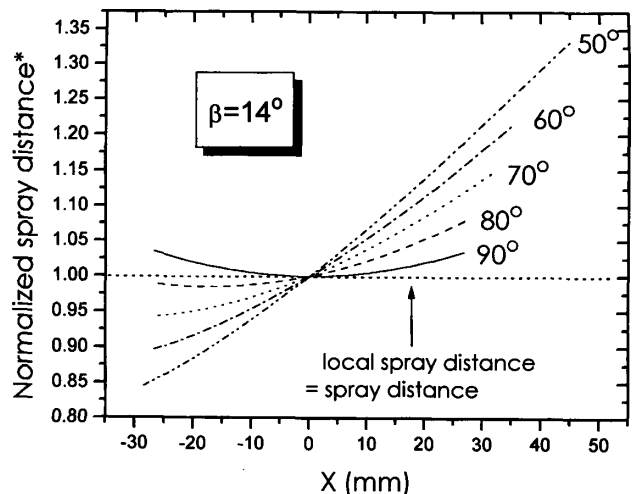


Fig. 6. Variation of local spray distance with different spray angles. *Normalized spray distance=local spray distance/spray distance.

Table 1

	Components	Content (w.%)	Minimum (%)	Maximum (%)
NiAl Powder	Aluminum	4.320	4.000	5.500
	Nickel	93.430	93.000	0.000
	Organic solids	2.200	0.000	2.500
	Others total	0.050	0.000	1.000
Cr ₃ C ₂ -NiCr powder				
Chromium carbide powder (75%)	Carbon	13.1	12.5	
	Silicon	0.08		0.10
	Chromium	86.14	85.50	
	Iron	0.23		0.70
Nickel chromium alloy (25%)	Carbon	0.01		0.25
	Manganese	0.88		2.50
	Silicon	1.00		1.50
	Chromium	20.09	18.00	22.50
	Nickel	77.89	76.00	80.00
	Iron	0.13		1.00

MFG. Co. Ltd.). The cut-off value and stylus transverse speed were 0.8 mm and 6 mm s⁻¹, respectively. The measurement range was 30 μm for NiAl coatings and 10 μm for Cr₃C₂-NiCr coatings.

3.3. Tensile adhesion test (TAT)

3.3.1. Test fixture

The tensile adhesion test (TAT) was based on ASTM C 633. [11] The disk-shaped coupons were glued to the usual TAT fixtures so that a tensile force could be applied to the coating. The configuration of the test was similar to that specified by ASTM C 633, except that the pull-off bar had an 8 mm (5/16 in) diameter hole through which a dowel pin passed instead of a tapped hole as specified by ASTM C633. Another distinction is that the pull-off bar is slightly longer (30.48 mm (1.2 in)) than that recommended by the ASTM standard (25.4 mm (1 in)). This pull-off bar would produce different test results (by -20% higher) from ASTM C 633 because of the different stress distribution near the testing area. [12,13] However, the test results are still valid for relative comparisons.

3.3.2. Specimen assembly

The test coupon was placed between the two pull-off bars and attached using an adhesive. The surfaces of the pull-off bars and the test coupons (except the coating) were grit-blasted to enhance the adhesion of the epoxy. After curing, excess epoxy was removed using emery paper. Table 2 summarizes the test conditions.

Good alignment of the test assembly (two pull-off bars and the test coupon) was achieved by using a self-aligning jig during epoxy curing.

3.4. Microhardness test

Microhardness tests were performed using a **Micromet II®** (Buehler Ltd., Lake Bluff, Illinois) hardness tester. The measurement was made on the cross-section with one diagonal of the indenter parallel to the interface. The samples were polished using an **Automet®2/ Ecomet®3** automated polishing machine under the conditions shown in Table 3. The indenter load for the NiAl coating was 300 and 500 gf for the Cr₃C₂-NiCr coating. The duration of loading was 15 s for both materials. The indentations were applied near the center line of the coating thickness, and the distance between the indentations was at least three times the diagonal to prevent stress-field effects from nearby indentations.

3.5. Interfacial fracture toughness

An indentation technique was used to measure the interfacial critical strain energy release rate of the coatings. The applied load was 1 kgf and other test conditions and the sample preparations were the same as the microhardness test. The indentation was applied to the interface of the coating and the substrate with an indenter diagonal aligned with the interface.

3.6. Porosity

Optical image analysis (**Omnimet®1**, Buehler Ltd., Lake Bluff, Illinois) was used to measure the porosity of the coatings. The cross-sections of samples were polished with the conditions presented in Table 3. Ten frames were measured and then averaged for each sample.

Table 2

Test instrument and model no.	Hydraulic Instron (Instron Corp., Canton, MA), AW2414-1
Load cell capacity	200 kN
Crosshead speed	0.030 in min ⁻¹
Diameter of pull-off bar	25.4 mm (1 in)
Length of pull-off bar	30.5 mm (1.2 in)
Adhesive bonding agent	Liquid epoxy (Master Bond EP15, Hackensack, NJ)
Adhesive curing temperature	170 ± 6°C (340 ± 10°F)
Adhesive curing time	60 min, under pressure (about 0.3 MPa)

Table 3

Grinding	Time (min) ^a	Force, N sample ⁻¹ (lb sample ⁻¹)	rad s ⁻¹ (rpm)
240 grit SiC paper	3 [3]	13.3 (3)	25.1 (240)
45 μm diamond	3 [5]	22.2 (5)	25.1 (240)
9 μm diamond	5 [10]	22.2 (5)	8.4 (80)
3 μm diamond	6 [10]	22.2 (5)	12.6 (120)
0.05 μm alumina	3 [5]	22.2 (5)	12.6 (120)

^aThe bracketed numbers are for Cr₃C₂-NiCr coatings, and the unbracketed data are for NiAl.

4. Results and discussion

4.1. Porosity

The porosity increased from 2.1 to 4.5% for Cr₃C₂-NiCr and from 2.5 to 4.2% for NiAl when the spray angle changed from 90 to 50° (Fig. 9). The porosity of Cr₃C₂-NiCr coatings was more sensitive to the spray angle, with significant changes occurring at 70° compared to a lower angle of 60° for the NiAl feedstock porosity. The decrease in porosity was partly because the Y component of particle momentum (Fig. 7), as explained in Section 2, decreased with spray angle, i.e. higher impacting momentum of molten particles produced a denser deposit. In addition, when the

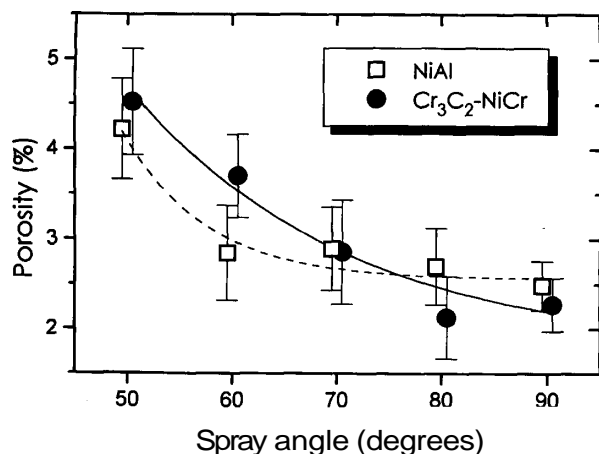


Fig. 9. Variation of porosity with spray angles.

particles impinge on the substrate at smaller angles the particles would not effectively cover the roughened surface of the substrate or previously deposited splats (i.e. a shadow effect). On the other hand, particles sprayed at 90° to the substrate covered the irregular contours more effectively.

Pore-size distributions were obtained using the Schwartz-Saltykov method [14,15]. Fig. 10 represents the pore size distribution of the two materials at five different spray angles. For Cr₃C₂-NiCr coatings, most of pores were within the range 0-2 μm, and for NiAl coatings 0-4 μm. The spray angle changed the pore size distribution of the Cr₃C₂-NiCr coating, i.e. spray angles less than 80° produced larger pores. The "shadow effect" accounts for the change in pore size distribution, i.e. it increases as the spray angle decreases, and therefore contributes to the larger pore size. The pore size increase is also attributed to the deviation of the local spray distance from the optimum condition, which leads to improper melting of particles and a smaller flattening degree of the impacting particles. NiAl coatings did not show notable changes in pore size distributions with spray angle.

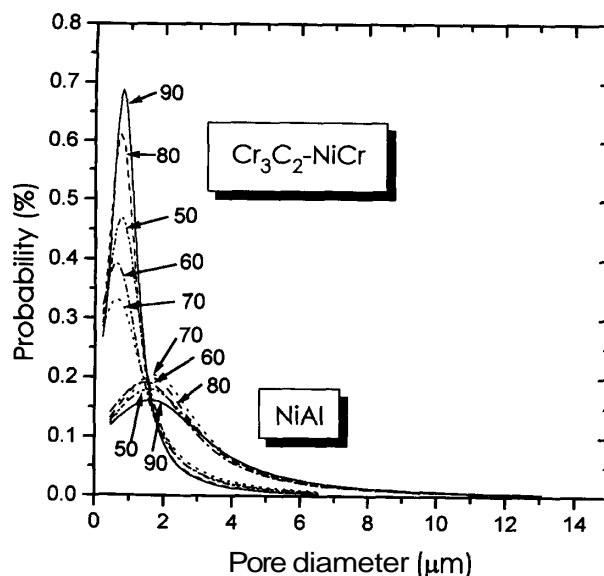


Fig. 10. Pore size distribution of Cr₃C₂-NiCr and NiAl for different spray angles.

4.2. Surface roughness

Fig. 11 shows the surface roughness of NiAl and $\text{Cr}_3\text{C}_2\text{-NiCr}$ coatings sprayed at various angles. The surface roughness was strongly dependent on the particle size of the sprayed powder (see Fig. 8), and was related to the porosity level. The surface roughness values of NiAl coatings tended to decrease as the spray angle increased. On the other hand, $\text{Cr}_3\text{C}_2\text{-NiCr}$ coatings showed no such trend with respect to spray angle.

4.3. Microhardness test

Fig. 12 illustrates the results of the microhardness tests of NiAl and $\text{Cr}_3\text{C}_2\text{-NiCr}$ coatings at five different spray angles. The $\text{Cr}_3\text{C}_2\text{-NiCr}$ coatings exhibited hardness values between 600 and 700 VHN, and the NiAl data were between 130 and 150 VHN. The mean value of hardness data of both coatings decreased slightly (9% decrease for $\text{Cr}_3\text{C}_2\text{-NiCr}$ and 8% for NiAl) when spray-

ing at angles of less than 90° . The data points of NiAl were more widely distributed than those of $\text{Cr}_3\text{C}_2\text{-NiCr}$ and the standard deviations of data did not show any dependence on spray angle (Table 4).

A Weibull analysis is a method of finding a parameter to assess the variability of the data and to index the reliability of materials. Fig. 13 compares Weibull plots of the two coatings with different spray angles. The Weibull moduli and the characteristic values for the two materials are listed in Table 4. The Weibull moduli exhibited no trends of change with spray angles and the values existed in quite narrow ranges.

The Weibull modulus (m), and the characteristic strength (X_0) can also be obtained using the maximum likelihood method; [16] and the values obtained are quite similar to the graphical method determined from the Weibull plot. The 90 and 95% confidence intervals of the Weibull moduli [15] are constructed in Fig. 14 and show that the Weibull moduli were essentially independent of spray angle. The Weibull modulus of 6–18 for NiAl coatings can be compared to 6.8–12.5 for a NiCoCrAlY bond coat [15]. The $\text{Cr}_3\text{C}_2\text{-NiCr}$ coatings exhibited high Weibull moduli; this was attributed to the hypersonic spraying process, whereas ceramic deposits normally exhibit values in the range of 4–6. The higher Weibull modulus of $\text{Cr}_3\text{C}_2\text{-NiCr}$ coatings compared to NiAl can be also inferred by the pore size distribution. Thus, the $\text{Cr}_3\text{C}_2\text{-NiCr}$ coating had a large number of smaller pores, whereas NiAl exhibited larger pores with a wider size distribution. The small area of the microhardness test (35–40 μm diagonal for $\text{Cr}_3\text{C}_2\text{-NiCr}$ and 60–70 μm diagonal for NiAl under the conditions used in the current study) examined only the properties of a limited area. Therefore, the more homogeneous $\text{Cr}_3\text{C}_2\text{-NiCr}$ coating resulted in higher Weibull modulus values.

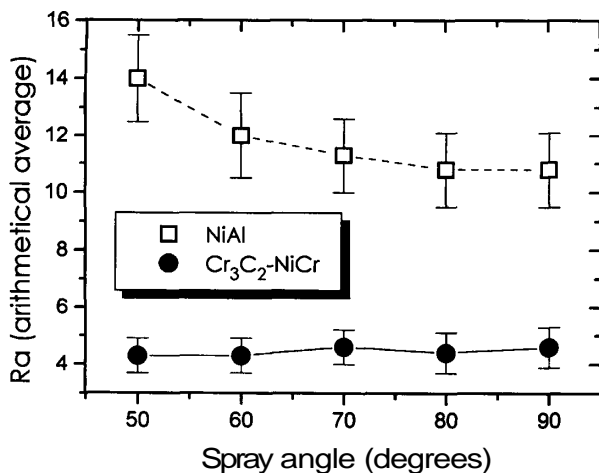


Fig. 11. Surface roughness of $\text{Cr}_3\text{C}_2\text{-NiCr}$ and NiAl coatings (μm).

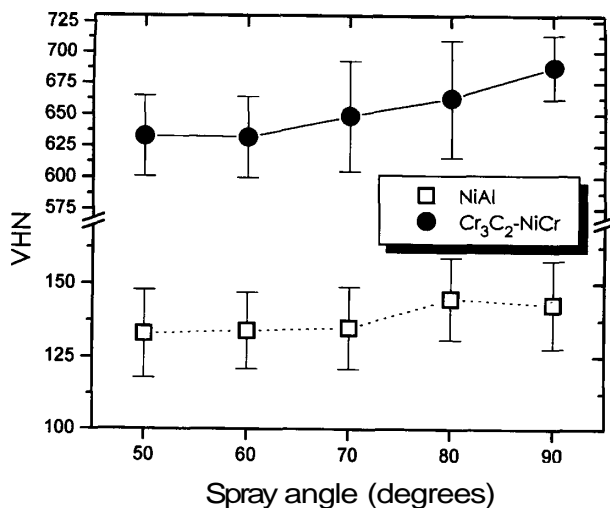


Fig. 12. Microhardness of $\text{Cr}_3\text{C}_2\text{-NiCr}$ and NiAl coatings.

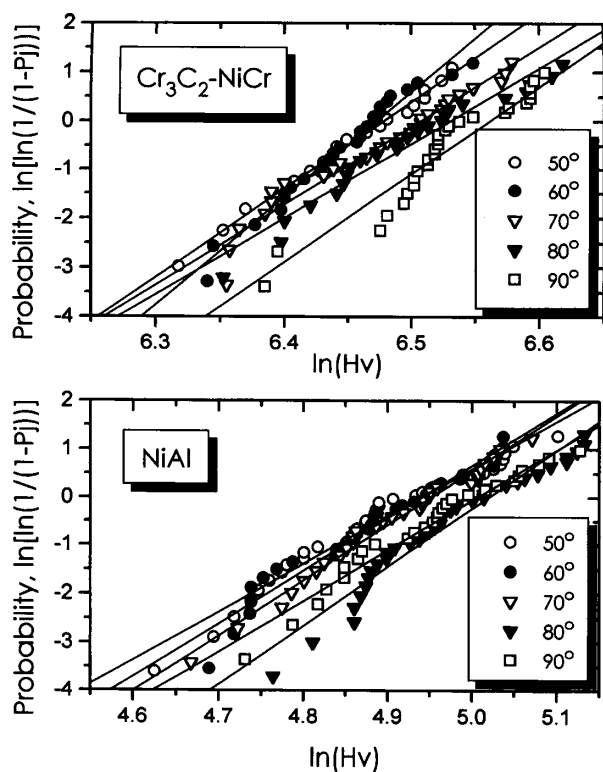
4.4. Interfacial critical strain energy release rate

The experimental results of interfacial critical strain energy release rate (\mathcal{G}_c) for NiAl and $\text{Cr}_3\text{C}_2\text{-NiCr}$ coatings on steel substrates are presented in Fig. 15. The \mathcal{G}_c values increased slightly with spray angle for both coatings, with the exception of the $\text{Cr}_3\text{C}_2\text{-NiCr}$ materials sprayed at 90° .

Weibull plots of interfacial fracture toughness for the two materials are presented in Fig. 16. NiAl coatings had slightly higher Weibull moduli than $\text{Cr}_3\text{C}_2\text{-NiCr}$ coatings. Spray angle did not influence the Weibull moduli, and high variance in data (up to 49%) was measured for both coatings (Table 5). Both materials exhibited low Weibull modulus values: 2.3–3.9 for $\text{Cr}_3\text{C}_2\text{-NiCr}$ coatings and 2.8–3.2 for NiAl coatings. The low Weibull moduli were attributed to the following causes. The contour of the interface between the coating and the substrates was irregular due to the grit-blasting prior to spraying, and it is difficult to align the indenter

Table 4

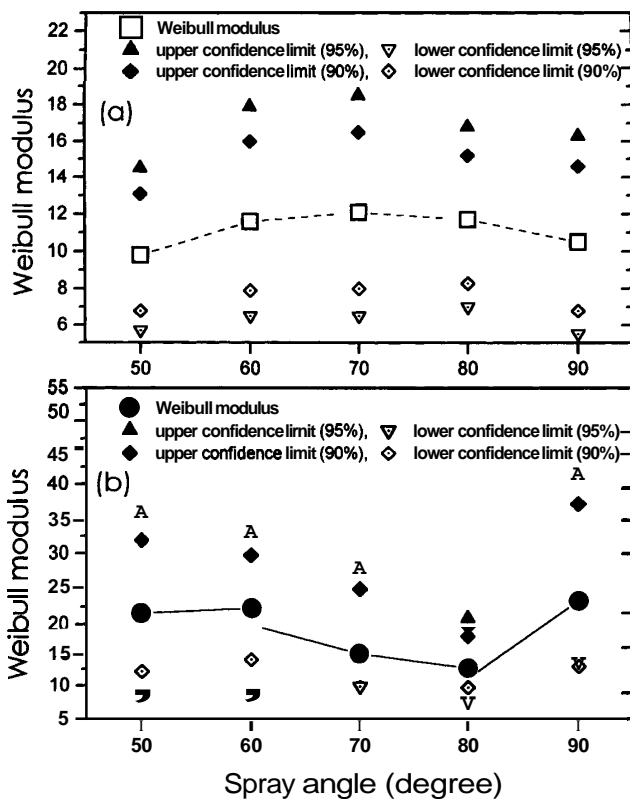
Material	Spray angle (°)	Number of tests	Mean (VHN)	Std. dev. (VHN)	Coefficient of variance (%)	Weibull modulus	Characteristic value (VHN)
Cr ₃ C ₂ -NiCr	50	19	633	32	5	18.0	650
	60	26	632	32	5	21.8	647
	70	28	649	44	7	16.2	669
	80	24	663	47	7	16.2	685
	90	29	687	41	6	18.0	706
NiAl	50	36	133	15	11	9.9	140
	60	34	134	13	10	11.0	140
	70	30	135	14	10	11.4	141
	80	40	145	14	10	12.1	151
	90	28	143	15	10	10.4	149

Fig. 13. Weibull plot of microhardness for Cr₃C₂-NiCr and NiAl coatings.

precisely to the interface because of the nature of the interface. In addition to the cracks at the interface originating from the indentation tip, many other cracks were observed near the indentation, which made interpretation difficult. Another distinction was that there are three types of crack path: (1) at the interface, (2) in the first or second layer of splats, or (3) both (1) and (2), which can be substantial factors in lowering the Weibull modulus.

4.5. Tensile adhesion test (TAT)

Fig. 17 shows the experimental results of TATs performed on NiAl and Cr₃C₂-NiCr coatings. The adhesion

Fig. 14. Confidence interval of Weibull moduli for (a) NiAl and (b) Cr₃C₂-NiCr coatings. Lines indicate the trend in the average Weibull modulus.

strength increased with spray angle: NiAl sprayed at 90° exhibited approximately 5% higher values than NiAl sprayed at 50°, and Cr₃C₂-NiCr at 90° was about 20% higher.

The mean fracture toughness from a TAT was converted to critical strain energy release rate (\mathcal{G}_{IC}) (Fig. 18). The \mathcal{G}_{IC} values ranged from 15.8 to 17.6 J m⁻² for NiAl coatings and from 16.8 to 23.7 J m⁻² for Cr₃C₂-NiCr and can be compared to those obtained from indentation tests (see Section 4.4,

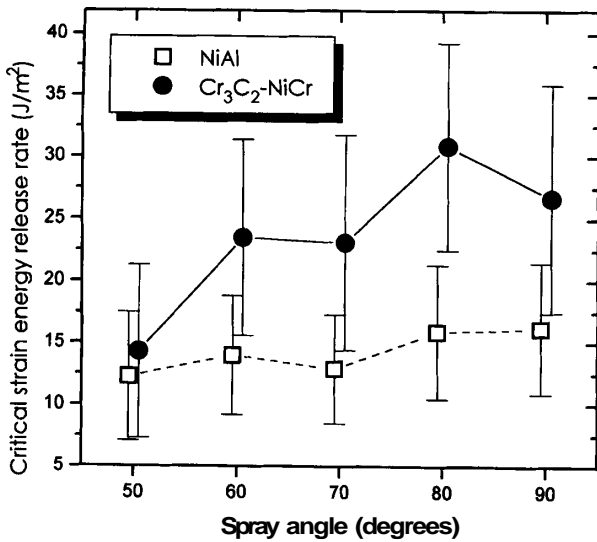


Fig. 15. Interfacial critical strain-energy release rate of Cr₃C₂-NiCr and NiAl coatings.

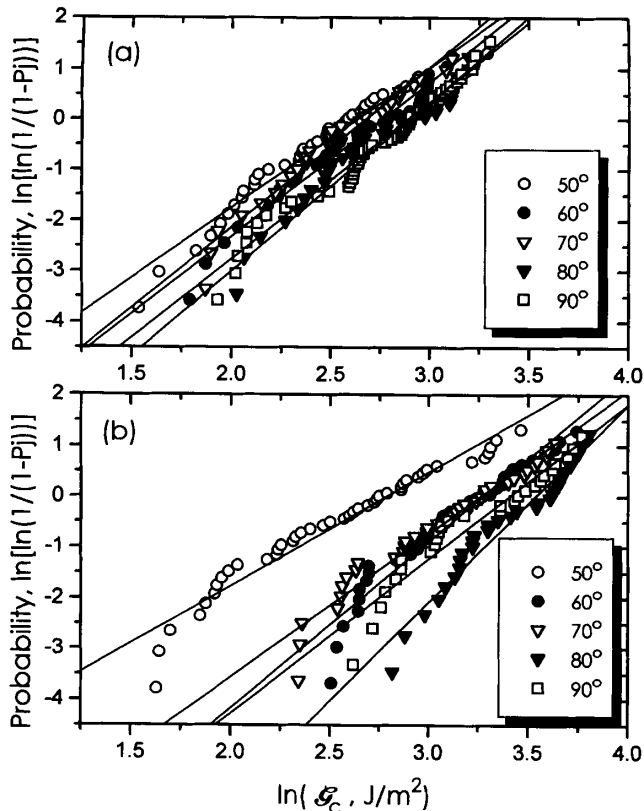


Fig. 16. Weibull plot of interfacial critical strain-energy release rate for (a) NiAl and (b) Cr₃C₂-NiCr coatings.

12.3–16.2 J m⁻² for NiAl and 14.3–30.9 J m⁻² for Cr₃C₂-NiCr.

The properties of thermal spray coatings are determined by several spray conditions. Spray angle has an influence on the mechanical properties: microhardness, adhesion strength and interfacial fracture toughness

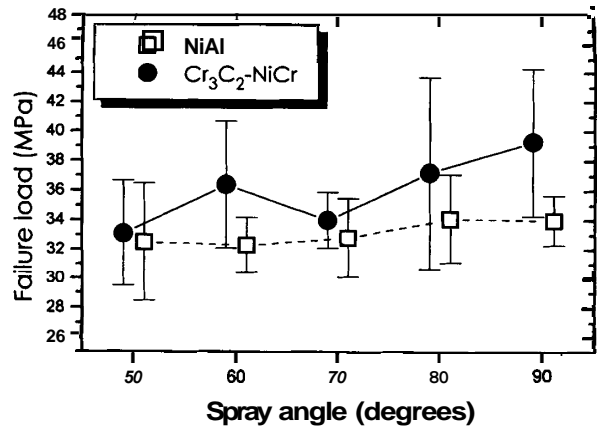


Fig. 17. TAT results of Cr₃C₂-NiCr and NiAl coatings.

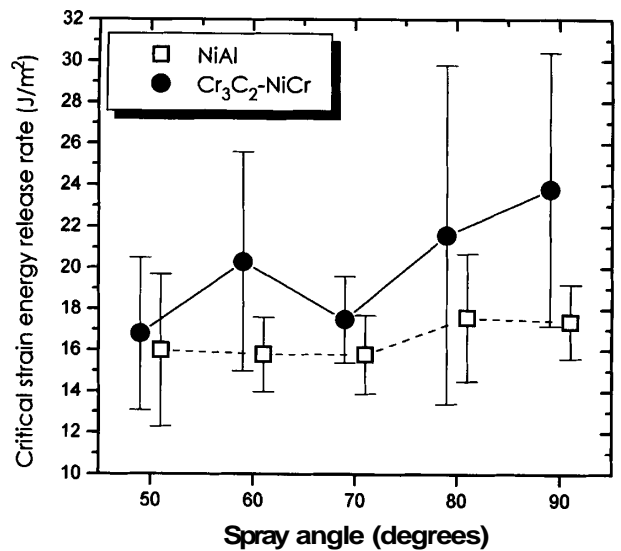


Fig. 18. Critical strain-energy release rate calculated from TAT data of Cr₃C₂-NiCr and NiAl coatings.

decreased with decreasing spray angles. By spraying at 90° denser structures with enhanced mechanical properties were achieved.

The influence of spray angle on the properties of deposits was attributed to the change in the local spray distance, and the impacting momentum. The local spray distance deviated from the optimum spray distance and this phenomenon became more pre-eminent as the spray angle decreased. The impacting momentum of the particle decreased with decreasing spray angle, which resulted in higher porosity and weaker bonding between lamellae (or between lamella and substrate).

5. Concluding remarks

The effects of spray angle on the thermal spraying process and the properties of thermal spray deposits of NiAl and Cr₃C₂-NiCr have been investigated. A simple

Table 5

Material	Spray angle (°)	Number of tests	Mean (J m ⁻²)	Std. dev. (J m ⁻²)	Coefficient of variance (%)	Weibull modulus	Characteristic value (J m ⁻²)
Cr ₃ C ₂ -NiCr	50	43	14.3	7.0	49	2.3	16.1
	60	39	23.5	7.9	34	3.3	26.3
	70	37	23.1	8.7	38	2.8	26.0
	80	31	30.9	8.4	27	3.9	34.2
	90	27	26.7	9.2	34	3.0	30.0
NiAl	50	41	12.3	5.2	42	2.8	13.8
	60	35	14.0	4.8	34	3.1	15.7
	70	28	12.9	4.4	34	3.2	14.4
	80	31	15.9	5.4	34	3.1	17.9
	90	54	16.2	5.3	33	3.1	18.1

mathematical model of deposit patterns at various spray angles has been formulated. The deposit pattern at a 90° spray angle was assumed to exhibit a Gaussian distribution. The deposit pattern deviated from the Gaussian distribution and the centroid of mass shifted to either side of the distribution as the spray angle decreased.

The porosity decreased with the spray angle for both materials. The surface roughness of NiAl was sensitive to spray angle, whereas Cr₃C₂-NiCr was not. The high porosity at low spray angles was attributed to the lower impacting momentum of particles as well as the low incident angle of particles impinging on the substrate. This phenomenon promoted conditions where the forming coating was less effective in covering the rough surface of the substrate or previously deposited particles.

The mechanical properties such as microhardness, adhesion strength and interfacial fracture toughness are altered by changes in the spray angle.

Acknowledgement

The authors would like to thank R. West and B. Palmieri (Howmet Corporation, 30 Corporate Drive North Haven, CT 06473) for sample preparation. The authors also wish to acknowledge S.M. Yi (Department of Mathematics, SUNY at Stony Brook) for his contribution to mathematical modeling of the spray print.

Appendix A

Derivation of general equation of distribution for spray angle α

The equation of a Gaussian distribution is:

$$P(x) = \frac{1}{\sqrt{\pi\sigma^2}} \exp\left[-\frac{(x-\mu)^2}{2\sigma^2}\right], \quad -\infty < x < \infty$$

In order to obtain a distribution equation on the x axis,

x should be transformed to x':

$$\frac{x}{x'} = \frac{\sin[90 - (\alpha - 0)]}{\sin(90 - \theta)} \quad (\text{A1})$$

Since $(90 - X) = \cos X$ and $\cos(X - Y) = \cos X \cos Y + \sin X \sin Y$:

$$\begin{aligned} \frac{x}{x'} &= \frac{\cos(\alpha - \theta)}{\cos \theta} = \frac{\cos \alpha \cos \theta + \sin \alpha \sin \theta}{\cos \theta} \\ &= \cos \alpha + \sin \alpha \tan \theta \end{aligned} \quad (\text{A2})$$

Therefore, if $\tan \theta$ is replaced by x/d and then (Eq. (A2)) is arranged for x:

$$x = \frac{dx' \cos \alpha}{d - x' \sin \alpha} \quad (\text{A3})$$

Substituting (Eq. (A3)) into (Eq. (1)) and setting $\mu = 0$:

$$P(x, \alpha) = \frac{1}{\sqrt{2\pi\sigma^2}} e^{-\frac{\left[\frac{dx \cos(90 - \alpha)}{d - x \sin(90 - \alpha)}\right]^2}{2\sigma^2}} \quad (\text{A4})$$

The function P is a probability function, and thus the integration of function P from $-\infty$ to $+\infty$ with regard to x should be 1, i.e.:

$$\int_{-\infty}^{\infty} P(x) dx = \int_{-\infty}^{\infty} P(x', \alpha) \frac{dx}{dx'} dx' = 1 \quad (\text{A5})$$

Meanwhile, the integration of $P(x', \alpha)$ with regard to x' is larger than 1. Therefore, a general equation for a certain spray angle $P'(x', \alpha)$ is obtained:

$$P'(x', \alpha) = P(x', \alpha) \frac{dx}{dx'} \quad (\text{A6})$$

After a simple calculation of $\frac{dx}{dx'}$, (Eq. (A6)) turns out

to be:

$$P'(x', \alpha) = \frac{1}{\sqrt{2\pi}\sigma} d^2 \times \frac{\cos(90-a)}{[d-x' \sin(\alpha)]^2} e^{-\frac{\left[\frac{dx' \cos(90-a)}{d-x' \sin(90-a)}\right]^2}{2\sigma^2}} \quad (\text{A7})$$

7.0.1. Calculation of standard deviation

To estimate the standard deviation of the Gaussian distribution, the concept of tolerance limit can be used. An interval covers a fixed portion of the population distribution with a specified confidence, and the end point of such intervals are called tolerance limits. Tolerance intervals are of the form:

$$\bar{X} \pm C_{T,P}(n)s \quad (\text{A8})$$

where $C_{T,P}(n)$ is a constant which is determined so that the interval covers a certain percentage such as 90%, 95%, or 99% of the population with confidence y , s is a standard deviation, and \bar{X} is a mean. In this case \bar{X} is zero and the confidence limit can be considered as the perpendicular section of the cone at the substrate (line AB in Fig. 2), and thus the standard deviation can be calculated.

Appendix B

Background to interfacial fracture toughness measurement

Numerous techniques exist to obtain the fracture toughness or critical strain-energy release rate of materials [17-19]. The indentation test evaluates the interfacial fracture toughness of thermal spray coatings [20-22]. The Vickers indenter introduces a mechanically stable crack into the interface of the coating and the substrate. The resistance of crack propagation along the interface is considered to be a measure of adhesion, and is expressed as a fracture mechanics parameter such as critical strain-energy release rate or critical stress intensity factor. A Vickers indenter was directly applied to the interface of the coating and the substrate. The crack length was then measured to determine the critical strain energy release rate, \mathcal{G}_c . Special care was taken to place the indenter tip exactly on the interface and to align the indenter diagonal with the interface. According to Willis [23] the critical strain energy release rate \mathcal{G}_c is given by:

$$\mathcal{G}_c = \alpha \Phi(G_1, G_2, \nu_1, \nu_2) \Psi(E_1, E_2, H_1, H_2) \frac{a^4}{c^3} \quad (\text{A9})$$

with

$$\Phi(G_1, G_2, \nu_1, \nu_2) = \frac{b^2 - d^2}{b} (1 + 4k^2)$$

$$b = \frac{1 - \nu_1}{2\pi G_1} + \frac{1 - \nu_2}{2\pi G_2}$$

$$d = \frac{1 - G\nu_1}{4\pi G_1} - \frac{1 - 2\nu_2}{4\pi G_2}$$

$$k = \frac{1}{2\pi} \ln \left[\frac{b+d}{b-d} \right]$$

$$\Psi(E_1, E_2, H_1, H_2) = \frac{1}{\left[\frac{1}{E_1} + \frac{1}{E_2} \right]^2} \frac{1}{\left[\sqrt{\frac{E_1}{H_1}} + \sqrt{\frac{E_2}{H_2}} \right]^2}$$

where H_1 and H_2 are hardness, G_1 and G_2 are the shear elastic moduli, ν_1 and ν_2 are the Poisson's ratios of the two materials, E_1 and E_2 are the Young's moduli of the coating, a and c are indentation impression and crack length, respectively, α is a constant independent of the system indenter and specimen. In this case α is 0.0197.

Appendix C

Background to fracture toughness calculation from TAT data

TAT data can be used to calculate the fracture toughness of thermal spray coatings. The specimen configuration of the TAT is regarded as a circumferentially cracked bar and the results can be analyzed in a same way as a fracture toughness test. The stress analysis from this type of specimen was conducted by Bueckner [24] and the fracture toughness is given by:

$$K_{IC} = P_c \times [-1.27 + 1.72(D/d)] \times D^{-3/2}$$

and

$$0.4 \leq d/D \leq 0.9$$

where K_{IC} is the fracture toughness ($\text{N m}^{-3/2}$), P_c is the fracture force (N), D is the outside diameter of the bar (2.54×10^{-2} m), an d is the inside diameter in the circumferentially notched bar (m).

References

- [1] M.M. Fasching, F.B. Prinz and L.E. Weiss, *J. Thermal Spray Technol.*, 2 (1993) 45.
- [2] A. Hasui, S. Kitahara and T. Fukushima, *Trans. Nat. Res. Inst. Metals*, 12 (1970) 9.
- [3] R.C. Tucker, Jr. and M.O. Price, *Proc. Int. Symp. on Advanced Thermal Technology and Allied Deposits (ATTAC)*, Osaka, Japan, 13-15 May, 1988, p. 61.

- [4] W.D. Swank, J.R. Fincke and D.C. Haggard, *Proc. 5th National Thermal Spray Conference*, ASM International, Anaheim, CA, 7–11 June, 1993, p. 25.
- [5] G. Montavon, C. Coddet, S. Sampath, H. Herman and C.C. Berndt, *Proc. 7th National Thermal Spray Conference*, ASM International, Boston, MA, 20–24 June, 1994, p. 469.
- [6] M.F. Smith, R.A. Neiser and R.C. Dykhuizen, *Proc. 7th National Thermal Spray Conference*, ASM International, Boston, MA, 20–24 June, 1994, p. 603.
- [7] L. Bianchi, A. Geirnaud, F. Blein, P. Lucchese and P. Fauchais, *J. Therm. Spray Technol.*, 4 (1995) 59.
- [8] S.J. Yankee and B.J. Pletka, *J. Therm. Spray Technol.*, 2 (1993) 271.
- [9] M. Vardelle, A. Vardelle, P. Fauchais and M.I. Boulos, *AIChE J.*, 29 (1983) 236.
- [10] ANSI B46.1-1978, *Surface Texture*, The American Society of Mechanical Engineers, New York, 1978.
- [11] ASTM C633-79, *Standard Test Method for Adhesion or Cohesion Strength of Flame Sprayed Coatings*, American Society for Testing and Materials, Warrendale, PA, 1992.
- [12] S.H. Leigh and C.C. Berndt, *J. Thermal Spray Technol.*, 3 (1994) 184.
- [13] W. Han, E.F. Rybicki and J.R. Shadley, *Proc. 13th International Thermal Spray Conference*, ASM International, Orlando, FL, 28 May – 5 June, 1992, p. 911.
- [14] E.E. Underwood, in R.T. DeHoff and F.N. Rhines (Eds.), *Quantitative Microscopy*, McGraw-Hill, New York, 1968, p. 149.
- [15] E.E. Underwood, *Quantitative Stereology*, Addison-Wesley, Reading, MA, p. 119.
- [16] C.K. Lin and C.C. Berndt, *J. Mater. Sci.*, 30 (1995) 111.
- [17] G.R. Anstis, P. Chantikul, B.R. Lawn and D.B. Marshall, *J. Am. Ceram. Soc.*, 64 (1981) 533.
- [18] S.D. Brown, B.A. Chapman and G.P. Wirtz, *Proc. 2nd National Thermal Spray Conference*, ASM International, Cincinnati, OH, 24–28 October, 1988, p. 147.
- [19] C.C. Berndt, in S.R. Valluri, D.M.R. Taplin, P. Rama Rao, J.F. Knott and S. Dubey (Eds), *Advances in Fracture Research*, Vol. 4, Pergamon, Oxford, 1984, p. 2545.
- [20] D. Choulier, P. Fluzin and C. Coddet, *Proc. 6th International Conference on Heat Treatment of Metals*, ASM International, Chicago, IL, 28–30 September, 1988, p. 75.
- [21] D. Choulier and C. Coddet, *Proc. 12th International Conference on Thermal Spraying*, London, 4–9 June, 1989, Paper No. 45.
- [22] R. Dal Maschio, V.M. Sgavo, F. Rigoni, L. Beramini and E. Galvanetto, *Proc. 13th International Thermal Spray Conference*, ASM International, Orlando, FL., 28 May – 5 June, 1992, p. 947.
- [23] J.R. Willis, *J. Mech. Phys. Solids*, 19 (1971) 353.
- [24] H.F. Bueckner, *Fracture Toughness Testing and Its Applications*, ASTM STP 381, American Society for Testing and materials, Philadelphia, PA, 1965, p. 85.